24th COBEM - 2017

24th ABCM International Congress of Mechanical Engineering
December 3-8, 2017, Curitiba, PR, Brazil

COBEM-2017-2153
Turbulence-Radiation Interactions in a Spatially Developing Heated Jet

J.M. Armengol [a,b]
jan@fem.unicamp.br
R. Vicquelin [b]
ronan.vicquelin@ecp.fr
A. Coussement [c]
axcousse@ulb.ac.be
R.G. Santos [a]
roger7@fem.unicamp.br
O. Gicquel [b]
olivier.gicquel@ecp.fr

[a]Faculty of Mechanical Engineering, University of Campinas (UNICAMP), Campinas-SP, Brazil
[b]Laboratoire EM2C, CNRS, CentraleSupélec, Université Paris-Saclay, 3, rue Joliot Curie, 91192 Gif-sur-Yvette cedex, France
[c]Université Libre de Bruxelles, Ecole Polytechnique de Bruxelles, Aero-Thermo-Mechanics Laboratory, Bruxelles, Belgium

Abstract. *This work studies the Turbulent Radiation Interactions (TRI) in a heated turbulent plane jet of water vapor discharging into a parallel low speed co-flow of cold water vapor. To this purpose, a comparison between the averaged radiative power from a coupled direct numerical simulation and the radiative power field when computed from the averaged temperature field is presented. This comparison allows a quantification of the TRI when turbulence is modelled by the Reynolds Average Navier-Stokes (RANS) technique. The radiative transfer equation is solved using a Monte Carlo Method and the Correlated K-distribution (CK) method is used to account for spectral dependency of the absorption coefficient.*

Keywords: *Turbulence-Radiation Interaction, Direct Numerical Simulation, Radiative Heat Transfer.*

1. INTRODUCTION

Numerical simulations have played a key role during the past decades in supporting the design stage in many industrial systems. However, the modelling of some complex systems involving multiple phenomena are still challenging problems for engineering and computational science. In applications such combustion systems or steam turbines, there is a strong coupling between thermal radiation and turbulence due to high operating temperature and pressure conditions. In such systems, despite the fact that radiation can be the dominant mode of heat transfer, radiation is often neglected or approximated by "gray" models or "optically thin" assumption. These simplistic approaches are usually driven by the increase in complexity and in time processing.

During the past decades, there has been a growing interest on the role of radiation in high temperature turbulent flows. For example, Mazumder and Modest (1999) have shown that neglecting radiation in a methane-air diffusion flame entails a decrease of about 250 K in the temperature field, on average. While using a simplistic approach for radiation, such as "gray" models or the "optically thin" assumption, leads to *underprediction* of up to 100 K (Modest and Haworth (2016)).

In the every-day industry applications, turbulence flow is modelled aiming to obtain good commitment between time processing and accuracy. Most of those models are based on averaged (RANS) values of the flow variables. Thus, fluctuations of velocity (u_i'), temperature (T') and species concentration (Y_k') are not directly resolved. Unfortunately, those fluctuations affect the radiation field since the emission ($\kappa_\eta I_{b,\eta}$) and absorption of radiation ($\kappa_\eta I_\eta$) are highly non-linear functions of temperature and species concentration. Here, κ_η stands for the spectral absorption coefficient which depends on the wavenumber η.

When a radiative energy balance is performed in the RANS context, the Radiative Transfer Equation (RTE) is averaged, and the non-resolved fluctuations can play an important role. The averaged form of the RTE in an emitting-absorbing and non-scattering medium on a specific direction defined by the unit vector s can be expressed as:

$$\frac{d < I_\eta >}{ds} = - < \kappa_\eta I_\eta > + < \kappa_\eta I_{b,\eta} > \tag{1}$$

Averaged emission $< \kappa_\eta I_{b,\eta} >$ and averaged absorption $< \kappa_\eta I_\eta >$ are unclosed terms, since their computation from averaged and instantaneous values are not necessarily equal, that is:

$$< \kappa_\eta I_{b,\eta} >=< \kappa_\eta >< I_{b,\eta} > + < \kappa'_\eta I'_{b,\eta} > \tag{2}$$

$$< \kappa_\eta I_\eta >=< \kappa_\eta >< I_\eta > + < \kappa'_\eta I'_\eta > \tag{3}$$

where it is considered that the spectral absorption coefficient is a function of the local instantaneous values of temperature and species concentration, $\kappa_\eta(T, Y_k)$ (assuming constant pressure), and the spectral blackbody intensity is solely a function of the local temperature, $I_{b,\eta}(T)$. Moreover, the spectral radiative intensity computed through the RTE is a function of the temperature and species concentration fields $I_\eta(T, Y_k)$. The terms $< \kappa'_\eta I'_{b,\eta} >$ and $< \kappa'_\eta I'_\eta >$ in Eqs. 2 and 3 are the so called emission and absorption TRI, respectively.

This work compares the results of the averaged radiative heat transfer computed from instantaneous values of temperature with the non-coupled results of the radiative heat transfer computed from averaged temperature field. To this end, two simulations are performed. First, a reference solutions is obtained from DNS of a heated plane jet coupled with a radiative solver. After that, the averaged temperature field is used to compute a non-coupled solution of the radiative heat transfer. The comparison of those two simulations bring into light a quantification of TRI in the RANS context of a spatially developing heated jet. Previous studies focus on the role of TRI in a temporal jet assuming periodic boundaries (Roger *et al.* (2011)), in homogeneous isotropic turbulence (Roger *et al.* (2009, 2010)), in a planar channel flow (Gupta *et al.* (2009); Zhang *et al.* (2013b)) or in a mixing layer (Ghosh and Friedrich (2015)).

Section 2 describes the physical model under study and the computational tools used for the simulations. Section 3 presents (i) a validation of the DNS code for the case of the isothermal plane jet, (ii) temperature results of the heated plane jet from DNS coupled with the radiative solver, and finally (iii) a comparison between the averaged radiative power from the coupled simulation and the radiative power field when computed from the averaged temperature field. Since DNS directly determines the instantaneous field at all the turbulent scales, it contributes to a better understanding of TRI and allows a quantitative comparison of the unclosed TRI terms.

2. Computational Procedure

The physical configuration investigated in this study consists in a heated turbulent plane jet of water vapor ($T_1 = 860$ K) discharging into a parallel low speed co-flow of cold water vapor ($T_2 = 380$ K), this temperature range has been chosen based on typical values found in a steam turbine. An effective domain extension of 20h x 20h x 4h (in x-, y- and z- directions respectively) is considered to compute the statistics of the flow. Figure 1 shows a schematic representation of the jet of initial velocity U_1 and a width opening h, with a velocity co-flow U_2. The half width of the jet $y_{1/2}(x)$, in

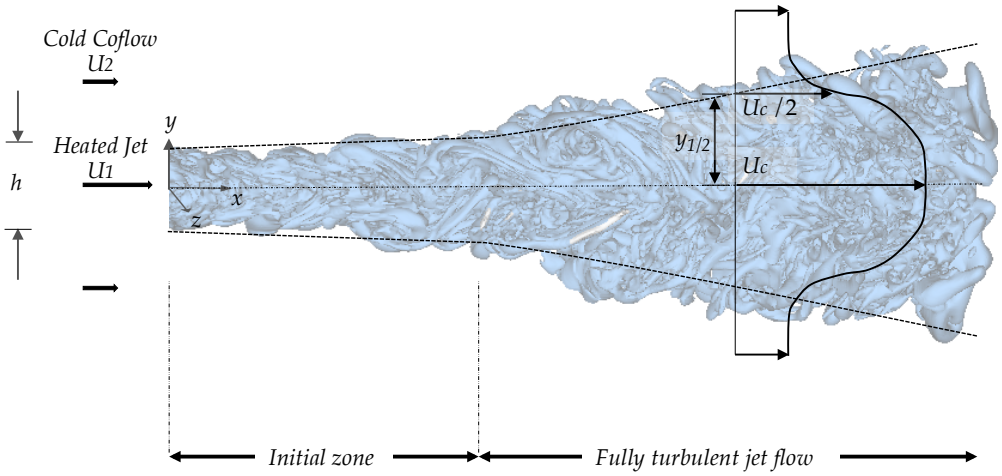

Figure 1: Schematic representation of a turbulent plane jet with a parallel co-flow.

which the velocity is half the velocity in the center of the jet U_c is also represented.

At the inlet boundary, we imposed a subsonic non-reflecting condition. The inlet velocity and temperature profiles are specified by the hyperbolic functions:

$$U_{in}(y) = \frac{U_1 + U_2}{2} + \frac{U_1 - U_2}{2} \tanh\left(\frac{h/2 - |y|}{2\theta}\right), \tag{4}$$

$$T_{in}(y) = \frac{T_1 + T_2}{2} + \frac{T_1 - T_2}{2} \tanh\left(\frac{h/2 - |y|}{2\theta}\right), \tag{5}$$

where U_1 and U_2 are the jet and co-flow velocities, the ratio between velocities is set to be $U_2/U_1 = 0.1$, and $\theta = 3.5{\cdot}10^{-2}$ is the shear layer momentum thickness. The Reynolds number based on the width opening h is set to

$$Re = \frac{\rho \Delta U_0 h}{\mu} = 1500, \tag{6}$$

where $\Delta U_0 = U_1 - U_2$.

Since direct numerical simulations are expensive in terms of computational power, we aim to reduce the computational domain by injecting artificial turbulence at the jet region in the inlet boundary. In doing so, turbulent instabilities are promoted, increasing the rate at which the jet reaches self-similarity, and thus saving a considerable amount of time processing.

A turbulent field is generated using a Passot Pouquet model which defines the turbulent kinetic energy spectrum $E(k)$, being k the wavenumber $k = 2\pi/\lambda$ and λ the wavelength. Such a model is usually used for low Reynolds number since it well describes the largest turbulent scales (k_e) but it does not represent the smallest turbulent structures (Passot and Pouquet (1987)). The Passot Pouquet model computes the turbulent kinetic energy spectrum as :

$$E(k) = A \left(\frac{k}{k_e}\right)^4 exp\left[-2\left(\frac{k}{k_e}\right)^2\right], \tag{7}$$

where A is an independent variable of k defined by $A = \frac{16n}{3}\frac{u'^2}{k_e}\sqrt{2/\pi}$. Here, u' stands for the *turbulent velocity* and n is the number of dimensions, both are risen from the definition of the turbulent kinetic energy (K) :

$$K = \frac{1}{2}\langle u_i' u_i' \rangle = \frac{n}{2} u'^2. \tag{8}$$

Following the implementation of Caudal (2013) we define the turbulent kinetic energy spectrum by fixing the auto-correlation integral scale $L^i_{i,i}$ and the *turbulent velocity* u' to the values: $L^i_{i,i} = h/3$ and $u' = U_0/18$.

2.1 DNS numerical characteristics

The governing equations used to describe the dynamics of the plane jet are the compressible Navier-Stokes equations, which are discretized in space and time for its numerical solution. In order to assure high accuracy, a 4th order centred finite-difference scheme for the spatial derivatives and an explicit 4th order Runge-Kutta method to advance in time are used (Kennedy and Carpenter (1994)). An implicit filter of 8th order detailed in Gaitonde and Visbal (1999) is used for stability purposes. As described in Poinsot and Lele (1992) the inflow and outflow boundary conditions are formulated using the Navier-Stokes Characteristic Boundary Conditions (NSCBC), the bases of the implementation of NSCBC is described in Coussement *et al.* (2012a). A general description of the implementation can be found in the work of Coussement *et al.* (2012b), and the recent studies of Castela *et al.* (2016, 2017) also used this same code.

The Acoustic Speed Reduction method is applied in order to increase the time step and so reduce the computational power to achieve statistical convergence, a detailed study of this method can be found in the work of Wang and Trouvé (2004).

The grid is non-uniform in the x- and y- directions but it is uniform in the span-wise direction. The solution is computed using 500 x 350 x 112 grid points, in the x, y and z directions, respectively. Considering the Kolmogorov hypotheses $\eta \equiv \left(\frac{\nu^3}{\epsilon}\right)^{1/4}$ where ν is the kinematic viscosity and ϵ is the dissipation rate; knowing ν as a function of temperature and estimating ϵ from previous DNS results (Stanley *et al.* (2002)), the grid spacing is set to be locally at least four times the local Kolmogorov scale $\eta(x, y)$.

2.2 Radiative heat transfer

A Monte Carlo Method is used in order to compute the radiative heat transfer in a participating medium. This method consists on tracing the history of a statistically meaningful random sample of photons from their points of emission to their points of absorption, a general description of this method applied to radiative heat transfer in participating medium can be found in Modest (2013). Taking advantage of the reciprocity principle the Emission-based Reciprocity Monte Carlo

Method (ERM) is used. The details of the ERM method can be found in the work of Tessé *et al.* (2002). The spectral absorption coefficient of water vapor is computed by a Correlated k-distribution (CK) method (Taine and Soufiani (1999)). Additionaly, the pure random generator has been replaced for a pseudo-random generator based on the Sobol sequences (Joe and Kuo (2008)). This pseudo-random generator provides a faster convergence of the radiative solution, a discussion on the efficiencies of the pseudo-random generator and the ERM can be found in the work of Palluotto *et al.* (2017).

The grid to compute the radiative solution is based on the DNS mesh, but taking on each direction one point every two points. That way, the radiative solution uses half of the points in each direction leading to a mesh grid of 250x175x57 grid points in the x, y and z directions, respectively. Moreover, radiative power is only calculated at points $4y_{1/2}(x)$ or closer to the jet centerline in order to save computational power.

This Monte Carlo code has already been used in various studies such as Zhang *et al.* (2009, 2012); Zhang (2013); Zhang *et al.* (2013b,a), Koren (2016) and Palluotto *et al.* (2017).

The solution of the Monte Carlo solver is considered converged when a *rms* lower than 3 % of the mean radiative power is achieved. In regions where the mean radiative power is close to 0 and so the relative *rms* is hard to converge, an absolute value of the *rms* of 2000 W/m^3 is considered to achieve convergence. If those two criterions are not accomplish in a specific grid point a maximum of 10^5 rays departing from the point are considered.

The energy exchanged by radiation inside a control volume is the radiative power (P_{rad}) per unit volume which is the difference between emitted energy and absorbed energy:

$$P_{rad} = \kappa_\eta \left(-4\pi I_{b,\eta} + \int_{4\pi} I_\eta d\Omega \right) \tag{9}$$

In order to couple the radiative heat transfer with the flow field, P_{rad} acts a source terms in the energy transport equation of the flow field.

3. Results

In this section DNS results of an isothermal plane jet are compared with experimental and numerical results in order to validate the code. Then, results of the heated plane jet from DNS coupled with the radiative solver are shown. Finally, this section discusses a comparison between the averaged radiative power from the coupled simulation and the non-coupled radiative power field when computed from the averaged temperature field.

3.1 Isothermal plane jet

Before presenting averaged results from DNS, let us defined the time averaging or Reynolds averaging of a time-dependent quantity $f(t)$ as

$$\langle f \rangle = \frac{1}{t^*} \int_{t^*} f(t) dt, \tag{10}$$

where t^* is the time-averaged period, which should be much more larger than the characteristic time of the fluctuations. In this study the statistics are obtained averaging the data during approximately 6 flow time units, defined as:

$$\frac{t^*(U_1 + U_2)}{2L_X} = 6 \tag{11}$$

where L_x is the domain size in the x direction and it is set to $20h$. Fluctuations are defined by:

$$f' = f - \langle f \rangle. \tag{12}$$

Defining $U_e = U - U_2$ as the averaged local velocity minus the co-flow velocity and $\Delta U_c = U_{y=0} - U_2$ as the averaged velocity at the centerline of the jet minus the co-flow velocity, the auto-similar profiles of vertical and horizontal averaged velocities are respectively presented in Fig. 2a and 2b. Results are compared with the experimental data of Gutmark and Wygnanski (1976), Deo *et al.* (2008) and the numeric results of Stanley *et al.* (2002).

Averaged velocity profiles of the isothermal plane jet are in good agreement with previous experimental and numerical works. Those results are here presented as a validation of the plane jet set up in the DNS code.

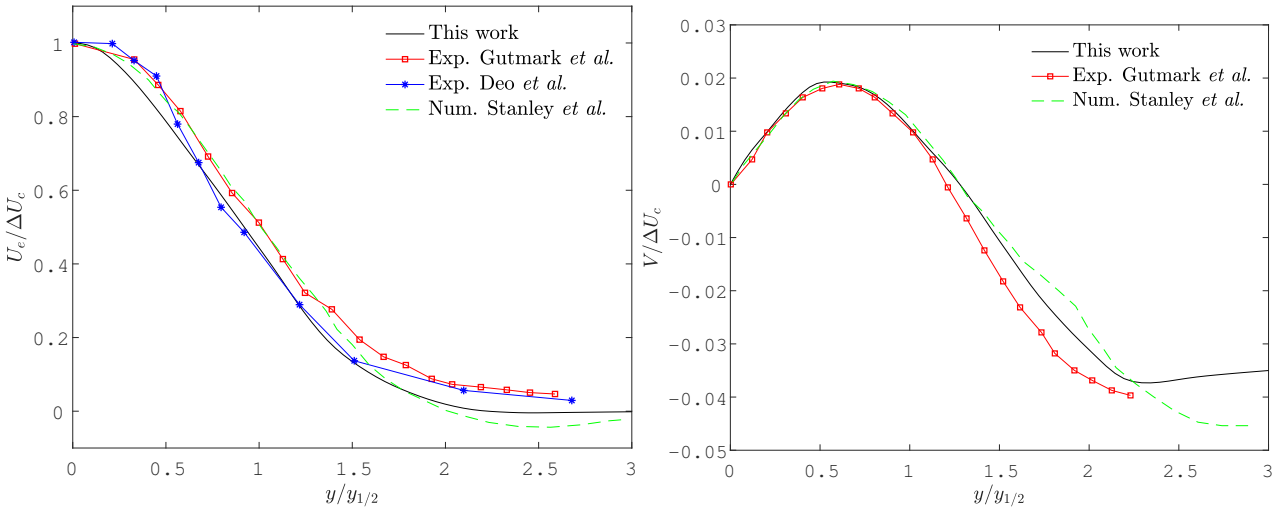

(a) (b)

Figure 2: Self-similar velocity profiles of (a) horizontal velocity and (b) vertical velocity.

3.2 Heated plane jet

The heated jet is set to a temperature of 860 K, while the temperature in the co-flow is set to 380 K, this temperature range has been chosen based on typical values found in a steam turbine. Figure 3 shows the isosurface of temperature 600K of a DNS coupled with the radiative solver of the heated plane jet.

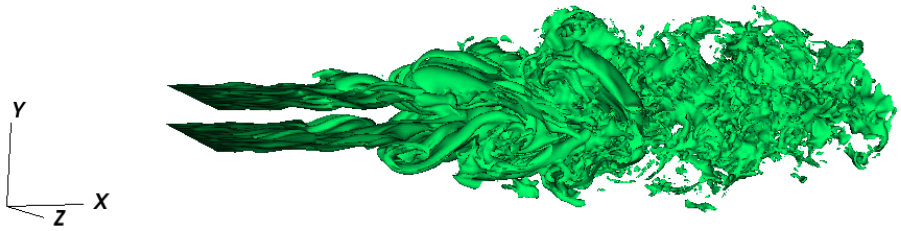

Figure 3: Isosurface of T=600 K of the heated plane jet with a parallel cold co-flow.

Figure 4 shows the averaged results of temperature and its fluctuations form the DNS solution dynamically coupled with the radiative solver, the procedure for the coupling follows previous works of Koren (2016); Zhang (2013). The temperature averaged field of Fig. 4a is used for the non-coupled radiative simulation in order to obtain the $P_{rad}(< T >)$ field. Figure 4b shows the averaged *rms* of temperature adimensionalized by the local temperature.

3.3 Radiative heat transfer computations of the heated plane jet

The results of the averaged radiative power $< P_{rad}(T) >$ from a dynamically coupled simulation of the DNS code together with the solution of the RTE are presented in Fig. 5a. On the other hand, Figure 5b shows the non-coupled results of the radiative power $P_{rad}(< T >)$ from the averaged temperature field (already presented in Fig. 4a). In both figures (5a and 5b) P_{rad} has been delimited to the range 10^4 to -10^4 W/m^3 for visualization purposes. The actual minimal and maximal values are respectively $-4.4264 \cdot 10^5$ and $5.5439 \cdot 10^4$ W/m^3 for $< P_{rad}(T) >$, and $-4.7782 \cdot 10^5$ and $5.4431 \cdot 10^4$ W/m^3 for $P_{rad}(< T >)$.

As expected, Fig. 5 shows that the centerline of the jet which is the hottest region of the flow lose heat by radiation. This radiation is further absorbed for the colder regions around the centerline of the jet, tending to 0 as the distance to the centerline increases.

In order to put in evidence TRI effects on P_{rad}, Fig. 6 shows the absolute difference between $< P_{rad}(T) >$ and $P_{rad}(< T >)$. Such a difference is also reflected in Fig. 7 in which cross-section profiles of $< P_{rad}(T) >$ and $P_{rad}(< T >)$ adimensionalized by the magnitude of the averaged radiative power at the jet centerline $| < P_{rad,c}(T) > |$ are shown for different values of x ($x = 8h$, $x = 12h$, $x = 14h$ and $x = 18h$). In Figure 7 it can be observed two main regions in each profile: the emission region between the centerline of the jet and approximately $1.5y_{1/2}$, and the absorption region

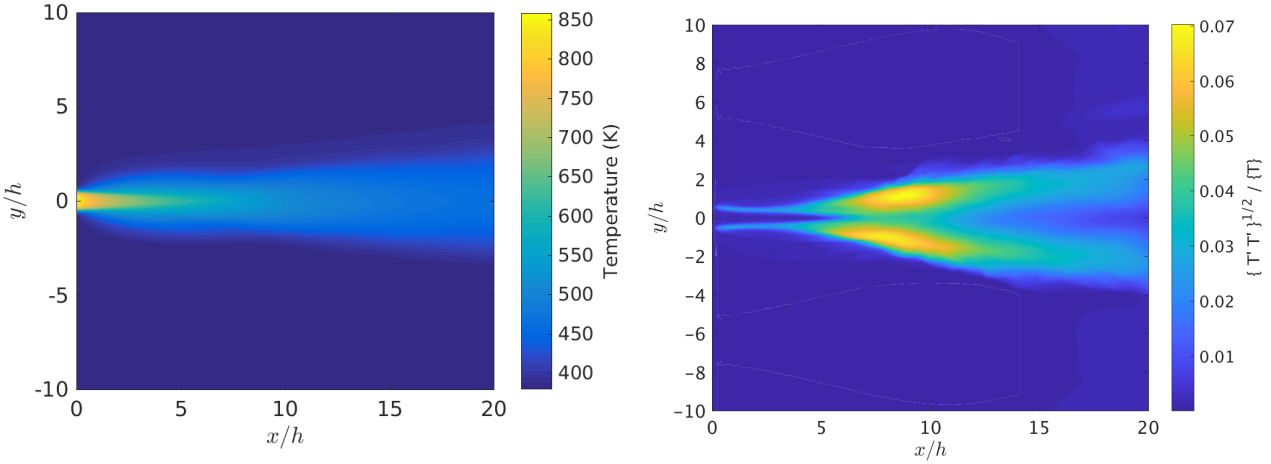

(a) (b)

Figure 4: (a) Averaged temperature field and (b) *rms* field of temperature

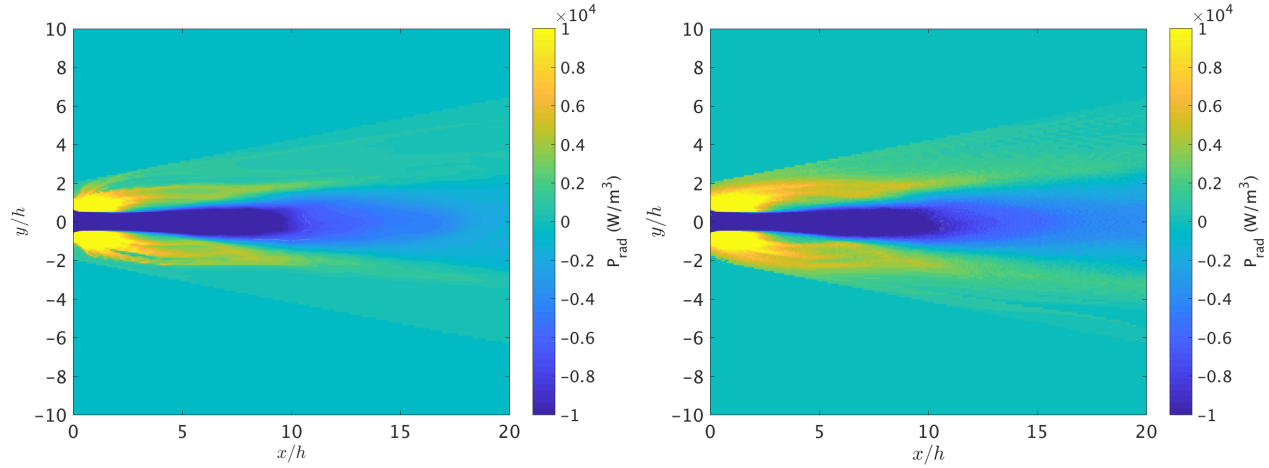

(a) (b)

Figure 5: Exchanged radiative power when computed as (a) $< P_{rad}(T) >$ and (b) $P_{rad}(< T >)$.

from $1.5y_{1/2}$ until the far-field in which P_{rad} tends to 0. The results show that both the emission and the absorption region are larger in module when P_{rad} is computed from the averaged temperature field.

Early works of Kabashnikov and Kmit (1979); Kabashnikov (1985) show that, for moderate optical thicknesses, the fluctuations of the radiative intensity are mainly caused by distant points. Thus, the correlation between the spectral intensity fluctuations and the local absorption coefficient fluctuations is negligible. This consideration is the so called optically thin fluctuation approximation (OTFA) and most of the works regarding TRI take advantage of it (Coelho (2007)). If the OTFA is assumed, TRI is mainly due to emission TRI. In the analytical effort of Snegirev (2004) the term $< \kappa_\eta(T) I_{b,\eta}(T) >$ is defined in terms of a development in Taylor series of the plank function and the absorption coefficient, together with some algebra and neglecting correlations higher than two, it is expressed as:

$$< \kappa_\eta(T) I_{b,\eta}(T) > \approx \kappa_\eta(< T >) I_{b,\eta}(< T >) \left(1 + 6 \frac{< T'^2 >}{< T >^2} + 4 \frac{< T'^2 >}{< \kappa >< T >} \frac{\partial \kappa_\eta}{\partial T}|_{<T>} \right), \tag{13}$$

where the correlation $< \kappa'_\eta T' > \approx < T'^2 > \frac{\partial \kappa_\eta}{\partial T}|_{<T>}$ if the fluctuations of the species concentration are ignored.

As discussed in Coelho (2007), the temperature fluctuations increase the radiation emitted by the medium, while the term $\frac{\partial \kappa_\eta}{\partial T}|_{<T>}$ can be positive or negative and so influences the role of the temperature fluctuations. Assuming the OTFA, the results of this study suggest that the term $\frac{\partial \kappa_\eta}{\partial T}|_{<T>}$ is negative leading to larger values on magnitude of P_{rad} when computed from the averaged temperature field. As a continuation of this work, it is expected to explicitly evaluate the term $\frac{\partial \kappa_\eta}{\partial T}|_{<T>}$ and to validate the OTFA for the current case in order to confirm these findings.

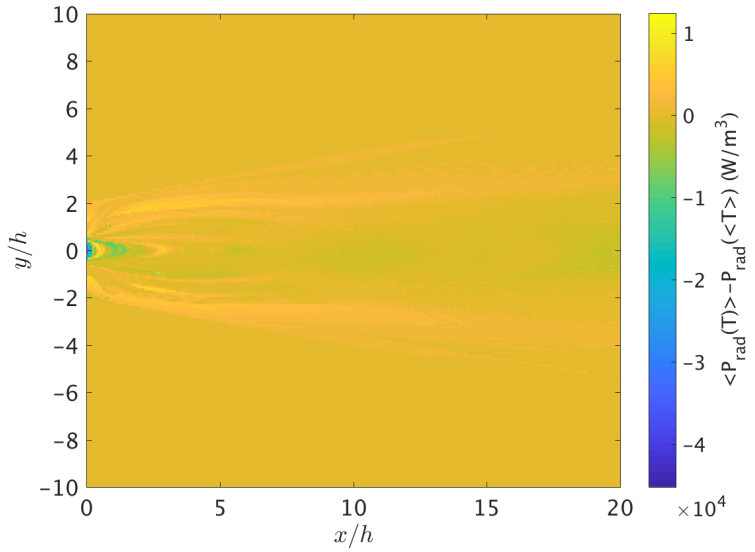

Figure 6: Absolute difference between $< P_{rad}(T) >$ and $P_{rad}(< T >)$

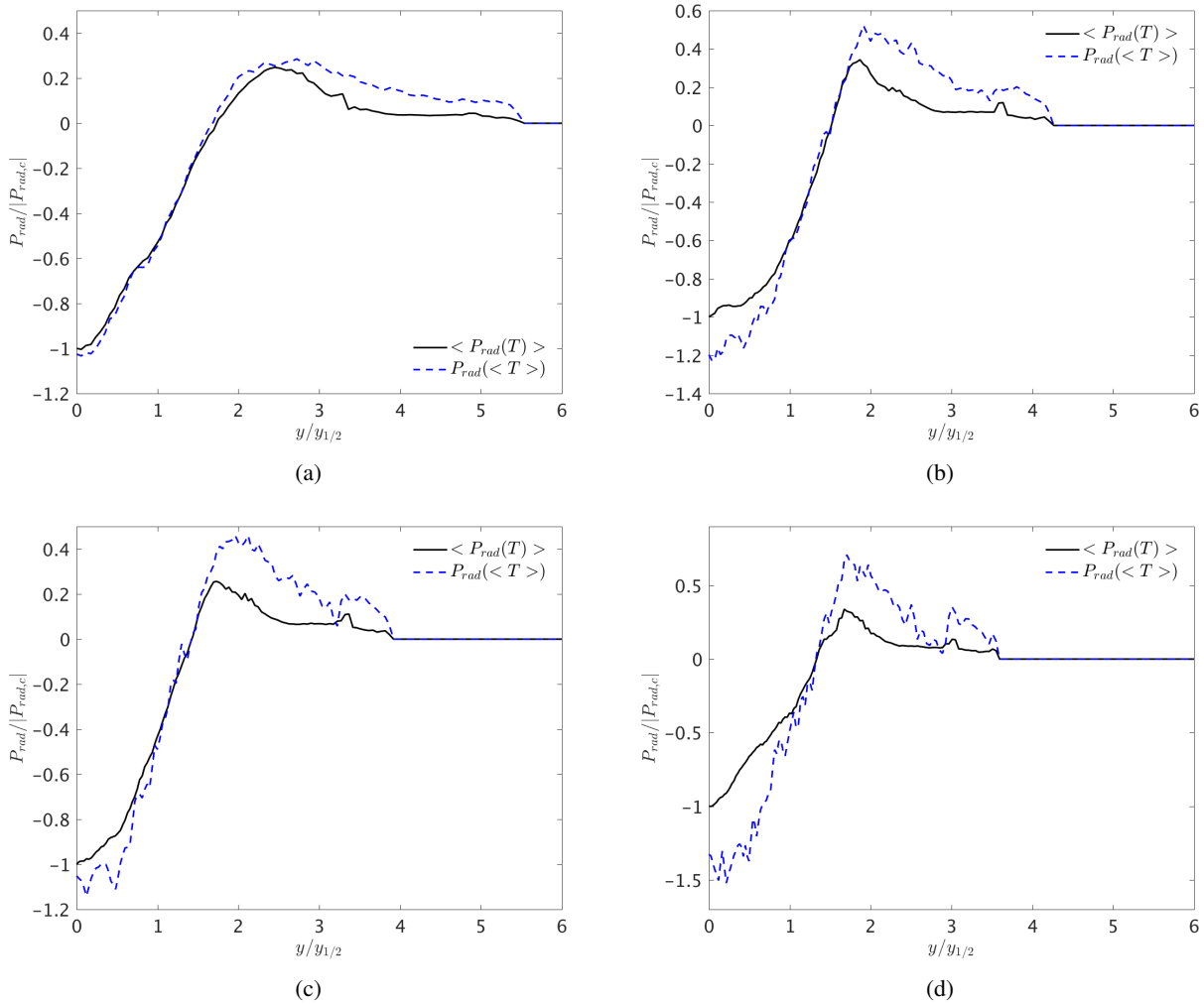

(a) (b)

(c) (d)

Figure 7: Cross section profiles of exchanged radiative power at (a) $x = 8h$, (b) $x = 12h$, (c) $x = 14h$ and (d) $x = 18h$.

Figures 8a and 8b show respectively the relative and absolute statistical deviation related to the Monte Carlo error. It can be note, when compared to the averaged P_{rad} in Fig. 5 , that the larger values of the relative error are in points where P_{rad} is close to 0.

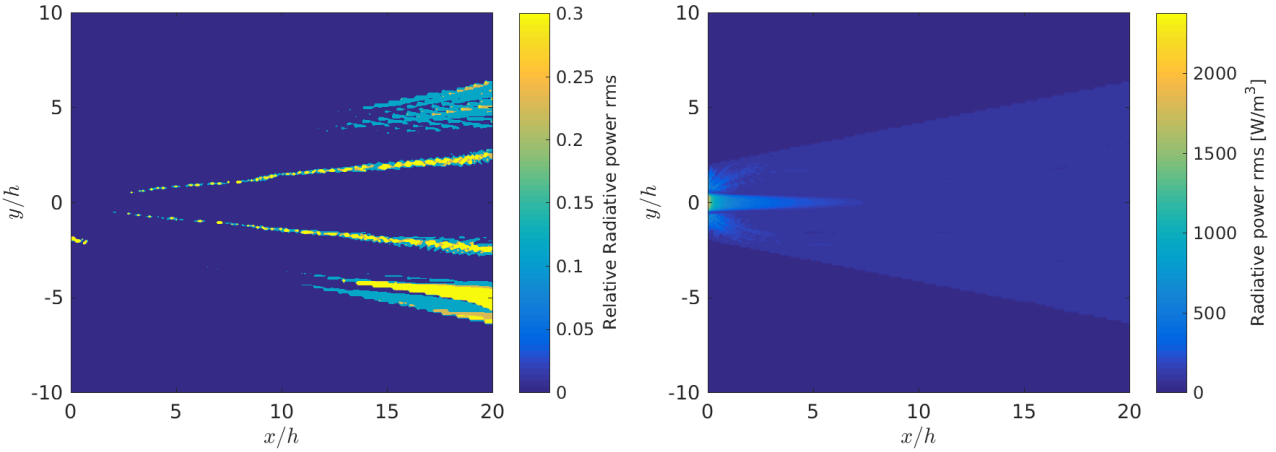

(a) (b)

Figure 8: Convergence of the radiative simulation: (a) relative *rms* of the radiative power and (b) absolute *rms* of the radiative power in W/m^3..

4. Conclusions

In this work a successful DNS of a heated plane jet coupled with a detailed radiative solver considering the spectral absorption coefficient of water vapor is obtained. Additionally, the averaged temperature field is used to compute a non-coupled solution of the radiative heat transfer. Those simulations allow comparing the so-called TRI effects on the P_{rad} as the difference between $< P_{rad}(T) >$ and $P_{rad}(< T >)$. It has been shown that TRI has a non-negligible effect on P_{rad}. Specifically, larger values on magnitude of P_{rad} are obtained when it is computed from the averaged temperature field. Those larger values together with the OTFA indicates that $< \kappa'_\eta T' >$ have negative values. Future works are planned to validate the OTFA for the current case and to explicitly evaluate the $< \kappa'_\eta T' >$ correlation.

5. REFERENCES

Castela, M., Fiorina, B., Coussement, A., Gicquel, O., Darabiha, N. and Laux, C.O., 2016. "Modelling the impact of non-equilibrium discharges on reactive mixtures for simulations of plasma-assisted ignition in turbulent flows". *Combustion and Flame*, Vol. 166, pp. 133–147.

Castela, M., Stepanyan, S., Fiorina, B., Coussement, A., Gicquel, O., Darabiha, N. and Laux, C.O., 2017. "A 3-d dns and experimental study of the effect of the recirculating flow pattern inside a reactive kernel produced by nanosecond plasma discharges in a methane-air mixture". *Proceedings of the Combustion Institute*, Vol. 36, No. 3, pp. 4095–4103.

Caudal, J., 2013. *Simulation numérique du reformage autothermique du méthane*. Ph.D. thesis, Ecole Centrale Paris.

Coelho, P.J., 2007. "Numerical simulation of the interaction between turbulence and radiation in reactive flows". *Progress in Energy and Combustion Science*, Vol. 33, No. 4, pp. 311–383.

Coussement, A., Gicquel, O., Caudal, J., Fiorina, B. and Degrez, G., 2012a. "Three-dimensional boundary conditions for numerical simulations of reactive compressible flows with complex thermochemistry". *Journal of computational physics*, Vol. 231, No. 17, pp. 5571–5611.

Coussement, A., Gicquel, O. and Degrez, G., 2012b. *Direct numerical simulation and reduced chemical schemes for combustion of perfect and real gases*. Ph.D. thesis, PhD thesis, Ecole Centrale des Arts et Manufactures (ECP).

Deo, R.C., Mi, J. and Nathan, G.J., 2008. "The influence of reynolds number on a plane jet". *Physics of Fluids*, Vol. 20, No. 7, p. 075108.

Gaitonde, D.V. and Visbal, M.R., 1999. "Further development of a navier stokes solution procedure based on higher-order formulas". *Technical Paper 99-0557, AIAA Press*.

Ghosh, S. and Friedrich, R., 2015. "Effects of radiative heat transfer on the turbulence structure in inert and reacting mixing layers". *Physics of Fluids*, Vol. 27, No. 5, p. 055107.

Gupta, A., Modest, M.F. and Haworth, D.C., 2009. "Large-eddy simulation of turbulence-radiation interactions in a turbulent planar channel flow". *Journal of Heat Transfer*, Vol. 131, No. 6, p. 061704.

Gutmark, E. and Wygnanski, I., 1976. "The planar turbulent jet". *Journal of Fluid Mechanics*, Vol. 73, No. 03, pp. 465–495.

Joe, S. and Kuo, F.Y., 2008. "Constructing sobol sequences with better two-dimensional projections". *SIAM Journal on Scientific Computing*, Vol. 30, No. 5, pp. 2635–2654.

Kabashnikov, V., 1985. "Thermal radiation of turbulent flows in the case of large fluctuations of the absorption coefficient

and the planck function". *Journal of Engineering Physics and Thermophysics*, Vol. 49, No. 1, pp. 778–784.

Kabashnikov, V. and Kmit, G., 1979. "Influence of turbulent fluctuations on thermal radiation". *Journal of Applied Spectroscopy*, Vol. 31, No. 2, pp. 963–967.

Kennedy, C.A. and Carpenter, M.H., 1994. "Several new numerical methods for compressible shear-layer simulations". *Applied Numerical Mathematics*, Vol. 14, No. 4, pp. 397–433.

Koren, C., 2016. *Modeling conjugate heat transfer phenomena for multi-physics simulations of combustion applications*. Ph.D. thesis, Paris Saclay.

Mazumder, S. and Modest, M.F., 1999. "A probability density function approach to modeling turbulence–radiation interactions in nonluminous flames". *International Journal of Heat and Mass Transfer*, Vol. 42, No. 6, pp. 971–991.

Modest, M.F., 2013. *Radiative heat transfer*. Academic press.

Modest, M.F. and Haworth, D.C., 2016. *Radiative Heat Transfer in Turbulent Combustion Systems: Theory and Applications*. Springer.

Palluotto, L., Dumont, N., Rodrigues, P., Koren, C., Vicquelin, R. and Gicquel, O., 2017. "Comparison of monte carlo methods efficiency to solve radiative energy transfer in high fidelity unsteady 3d simulations". In *ASME Turbo Expo 2017: Turbomachinery Technical Conference and Exposition*. American Society of Mechanical Engineers, pp. V05AT20A004–V05AT20A004.

Passot, T. and Pouquet, A., 1987. "Numerical simulation of compressible homogeneous flows in the turbulent regime". *Journal of Fluid Mechanics*, Vol. 181, pp. 441–466.

Poinsot, T.J. and Lele, S., 1992. "Boundary conditions for direct simulations of compressible viscous flows". *Journal of computational physics*, Vol. 101, No. 1, pp. 104–129.

Roger, M., Coelho, P. and Da Silva, C., 2011. "Relevance of the subgrid-scales for large eddy simulations of turbulence–radiation interactions in a turbulent plane jet". *Journal of Quantitative Spectroscopy and Radiative Transfer*, Vol. 112, No. 7, pp. 1250–1256.

Roger, M., Coelho, P.J. and da Silva, C.B., 2010. "The influence of the non-resolved scales of thermal radiation in large eddy simulation of turbulent flows: A fundamental study". *International Journal of Heat and Mass Transfer*, Vol. 53, No. 13, pp. 2897–2907.

Roger, M., Da Silva, C.B. and Coelho, P.J., 2009. "Analysis of the turbulence–radiation interactions for large eddy simulations of turbulent flows". *International Journal of Heat and Mass Transfer*, Vol. 52, No. 9, pp. 2243–2254.

Snegirev, A.Y., 2004. "Statistical modeling of thermal radiation transfer in buoyant turbulent diffusion flames". *Combustion and Flame*, Vol. 136, No. 1, pp. 51–71.

Stanley, S., Sarkar, S. and Mellado, J., 2002. "A study of the flow-field evolution and mixing in a planar turbulent jet using direct numerical simulation". *Journal of Fluid Mechanics*, Vol. 450, pp. 377–407.

Taine, J. and Soufiani, A., 1999. "Gas ir radiative properties: from spectroscopic data to approximate models". *Advances in heat transfer*, Vol. 33, pp. 295–414.

Tessé, L., Dupoirieux, F., Zamuner, B. and Taine, J., 2002. "Radiative transfer in real gases using reciprocal and forward monte carlo methods and a correlated-k approach". *International Journal of Heat and Mass Transfer*, Vol. 45, No. 13, pp. 2797–2814.

Wang, Y. and Trouvé, A., 2004. "Artificial acoustic stiffness reduction in fully compressible, direct numerical simulation of combustion". *Combustion Theory and Modelling*, Vol. 8, No. 3, pp. 633–660.

Zhang, J., Gicquel, O., Veynante, D. and Taine, J., 2009. "Monte carlo method of radiative transfer applied to a turbulent flame modeling with les". *Comptes Rendus Mécanique*, Vol. 337, No. 6, pp. 539–549.

Zhang, Y., Gicquel, O. and Taine, J., 2012. "Optimized emission-based reciprocity monte carlo method to speed up computation in complex systems". *International Journal of Heat and Mass Transfer*, Vol. 55, No. 25, pp. 8172–8177.

Zhang, Y., Vicquelin, R., Gicquel, O. and Taine, J., 2013a. "A wall model for les accounting for radiation effects". *International Journal of Heat and Mass Transfer*, Vol. 67, pp. 712–723.

Zhang, Y., Vicquelin, R., Gicquel, O. and Taine, J., 2013b. "Physical study of radiation effects on the boundary layer structure in a turbulent channel flow". *International Journal of Heat and Mass Transfer*, Vol. 61, pp. 654–666.

Zhang, Y., 2013. *Coupled convective heat transfer and radiative energy transfer in turbulent boundary layers*. Ph.D. thesis, Ecole Centrale Paris.

6. RESPONSIBILITY NOTICE

The authors are the only responsible for the printed material included in this paper.